POLITECNICO

MILANO 1863

SCUOLA DI INGEGNERIA INDUSTRIALE
E DELL'INFORMAZIONE

Simulation of a LEO orbiting microsat on Simulink

MSc in Space Engineering

Authors:

10723712	Marcello Pareschi	(BSc Aerospace Engineering - Politecnico di Milano)
10836125	Daniele Paternoster	(BSc Aerospace Engineering - Politecnico di Milano)
10711624	Alex Cristian Turcu	(BSc Aerospace Engineering - Politecnico di Milano)
10884250	Tamim Harun Or	(BCs Aerospace Engineering - International Islamic University Malaysia)

Professor: Franco Bernelli Zazzera

Academic year: 2023-2024

Abstract

La presente relazione di prova finale intende dare una descrizione dell'endoreattore F-1 prodotto da Rocketdyne. Cinque di questi motori vennero installati sul primo stadio S-IC del vettore Saturn V che portò il primo uomo sulla luna. L'obiettivo di questo stadio era quello di portare il razzo ad una quota di 61 km, fornendo un $\Delta v \simeq 2300$ m/s. Questo primo requisito verrà mostrato attraverso un modello matematico che simula il volo dello stadio S-IC.

Di seguito verranno analizzati i principali sistemi per un singolo motore, partendo dal sistema di storaggio e alimentazione dei propellenti costituito dai serbatoi e dalla turbopompa, passando per il sistema di generazione di potenza che comprende il gas generator e la turbina. Passando dalla camera di combustione si arriva infine al sistema di espansione gasdinamico e allo studio del suo raffreddamento. Si provvederà inoltre a dare una descrizione qualitativa e quantitativa delle scelte progettuali applicate ai tempi.

La discussione dei processi di combustione del gas generator e della camera di spinta si basa su dati provenienti da simulazioni eseguite con i programmi CEAM e RPA.

Contents

1. Symbols

1.1. Analisi della missione

A_e $[m^2]$ area di efflusso totale
ϕ $[rad]$ angolo di traiettoria del razzo

1.2. Analisi della missione 2

A_e $[m^2]$ area di efflusso totale
ϕ $[rad]$ angolo di traiettoria del razzo

2. Requirements

	Assigned specification	Modifications	Motivation for modifications
Platform	Microsat	-	-
Attitude parameters	Euler angles	-	-
Sensor	Earth Horizon	Magnetic, Sun	Magnetic because of magnetorquers Sun because no eclipse during orbit
Actuator	3 magnetorquers	2 reaction wheels	Underactuation of magnetorquers

Table 1: Mandatory requirements for the project

3. Framework Analysis

3.1. Satellite characterization

The satellite design was inspired by ESAIL, a microsatellite developed by exactEarth in cooperation with ESA. ESAIL was primarily developed for ship targeting.[1] Two configurations of the satellite are implemented: the undeployed configuration for the detumbling phase and the extended configuration for the slew and tracking phase. The deployed configuration is modeled as a cubic central body of side 70 cm and four solar panels, modeled as rectangular bodies of dimensions $70 \times 70 \times 1$ cm. Solar panels are set along y_B axis of body frame $\mathcal{B}$ with the normal of surface parallel to z_B axis, as shown in Figure 1.
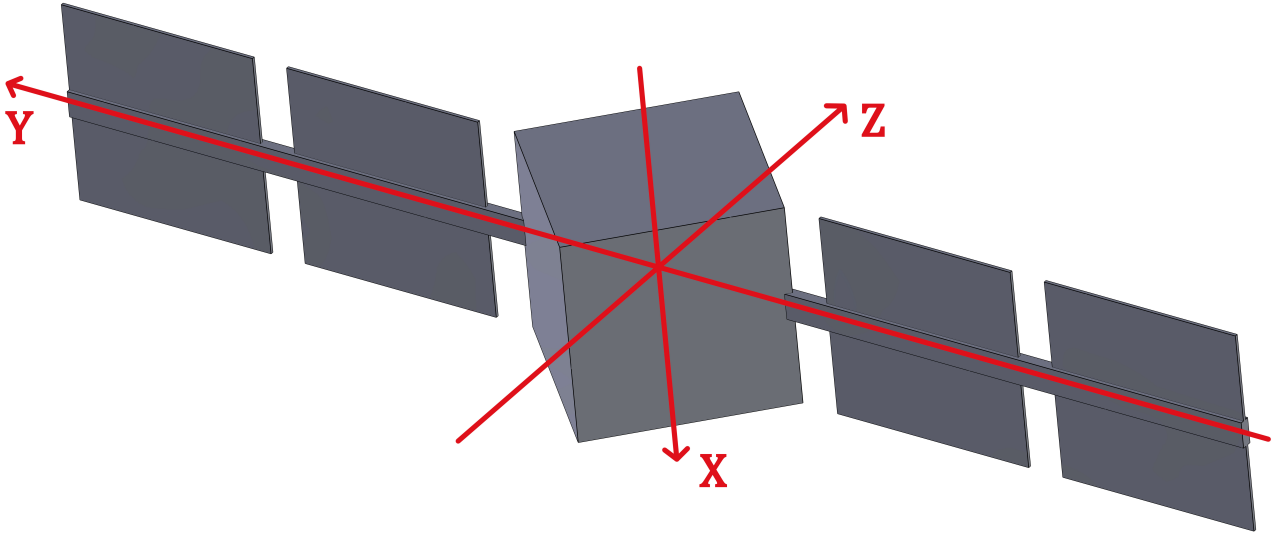
Figure 1: CAD model of the satellite

The mass is assumed to be 100 kg with isotropic distribution for simplicity. The inertia matrix results to be:

$$I = \begin{bmatrix} 22.9724 & 0 & 0 \\ 0 & 7.7770 & 0 \\ 0 & 0 & 23.1895 \end{bmatrix} \text{kg/m}^2 \tag{1}$$

The undeployed configuration is an isotropic cube of side 70 cm with the same mass. The inertia matrix of this undeployed configuration is then:

$$I = \begin{bmatrix} 8.1667 & 0 & 0 \\ 0 & 8.1667 & 0 \\ 0 & 0 & 8.1667 \end{bmatrix} \text{kg/m}^2 \tag{2}$$

3.2. Orbit characterization

The orbit adopted for the simulation is a nearly polar, LEO, Sun-synchronous orbit (SSO). Polar orbits allows to scan the whole globe during the several orbits thanks to Earth's rotation. SSO are orbits that maintain the same angle between their orbital plane and the direction that connects the Earth with the Sun[2]. This allows the spacecraft to monitor the Earth surface with the same conditions of light (or eventually darkness, if the plane is oriented in a certain way). Furthermore, a SSO can be selected to ensure constant visibility of the Sun.[3]

The data of the relation is based on the ephemeris of an ESAIL mission taken at 12:00 UT on December 16th, 2023. The orbit was then propagated using the simple two-body problem without any perturbations.

This is an approximation as several disturbances act on the satellite (as discussed in section 6). Using the ephemeris as the initial condition has the advantage of allowing the simulation of spacecraft motion in two or three periods of the orbit to be considered as Sun-synchronous. This is because the time of simulation is a snapshot compared to the time of action of the J2 effect responsible for the Sun-synchronous orbit, which is one year. Clearly, a more detailed simulation should consider the variation of the orbital parameters due to J2 and all the other perturbations.

The orbital parameters chosen as described above are the following:

$a\,[km]$	$e\,[-]$	$i\,[\deg]$	$\omega\,[\deg]$	$\Omega\,[\deg]$
6851	0.0018	97.40	101.58	0

Table 2: Orbital parameters
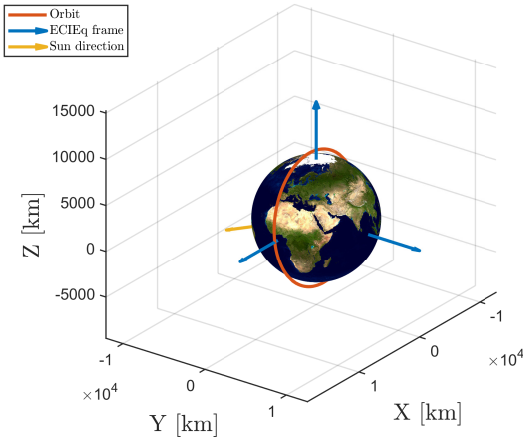
Figure 2: Orbit representation
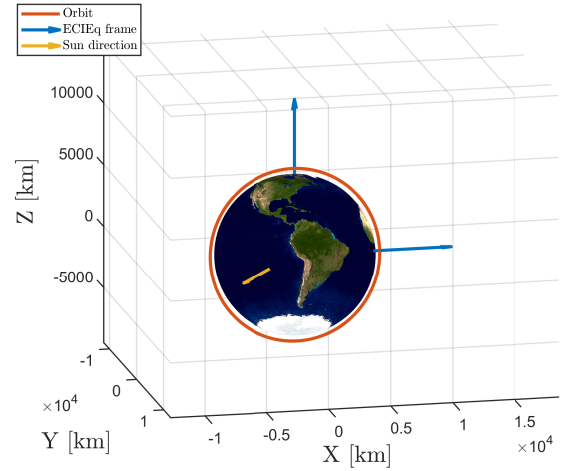
Figure 3: View from Sun direction

In Figure 2 and Figure 3 the Sun direction is plotted. It's easy to see that the orbit never goes into eclipse condition. On Simulink, the model implemented to retrieve the orbital position is based on the integration of the true anomaly:

$$\dot{\theta} = \frac{n\left(1 + e\cos\theta\right)^2}{\left(1 - e^2\right)^{3/2}} \tag{3}$$

Then, the radial distance is computed as:

$$r = \frac{a\left(1 - e^2\right)}{1 + e\cos\theta} \tag{4}$$

At this point it is easy to retrieve the position $\boldsymbol{r_P}$ of the satellite in the perifocal frame $\mathcal{P}$:

$$\boldsymbol{r_P} = r\begin{bmatrix}\cos\theta \\ \sin\theta \\ 0\end{bmatrix} \tag{5}$$

The position in the inertial frame $\mathcal{N}$ is calculated using the transpose of the rotation matrix $\boldsymbol{A_{PN}} = \boldsymbol{R_3}\left(\omega\right)\boldsymbol{R_1}\left(i\right)\boldsymbol{R_3}\left(\Omega\right)$:

$$\boldsymbol{r_N} = \boldsymbol{A_{PN}^T}\,\boldsymbol{r_p} \tag{6}$$

4. Dynamics

The equations of the dynamics adopted for the rotating rigid body motion are the Euler equations. The set of equations are referred to the principal axis frame of the satellite. This frame coincides with the body frame $\mathcal{B}$ previously defined (subsection 3.1). It is described by three unit vectors $\{x_B, y_B, z_B\}$ that are in the direction of principal inertia axis of the satellite.

$$I\dot{\omega} + \omega \times I\omega = M_d + M_c \tag{7}$$

In Equation 7 the external torque is split into two contributions. M_d describes the disturbance torques acting on the spacecraft due to environment, it is treated in more detail in section 6. M_c is referred to the control torque that the actuators generate in order perform the tasks required by the control logic (see section 10).

With particular reference to the Simulink model, the two different configurations of the satellite are considered: undeployed configuration for detumbling phase and extended configuration for slew and tracking. Since the inertia matrix of the system must switch from Equation 2 to Equation 1, a logic switch has been implemented during the simulation, using a flag based on the activation of the detumbling control. This istantaneous switch is not completely realistic since the extraction of the panels would require some finite time and could influence the real dynamic of the satellite. Anyhow, for the microsat considered, the retracted configuration allows a faster detumbling and also reduces the inertia loads and stresses on the solar panels and the structure.

5. Kinematics

As specified in section 2, the attitude parameters of the satellite are expressed through the use of Euler angles. The kinematics calculated according to this parameterization follows these steps:

• given the angular velocity ω from dynamics for each time and the initial condition on Euler angles s_0, compute the time derivatives of the angles $\dot{s}$;

• integrate the derivatives to obtain the set of Euler angles s for each time;

• from the calculated angles, compute the attitude matrix A.

When dealing with this type of parameterization, a major issue arises due to the singularity conditions on the second angle θ for any chosen set of three Euler angles. This can cause the derivatives of the other two angles to tend towards infinity. The problem is a result of the fact that, under these specific conditions, the set of Euler angles is not uniquely defined, as the first and third rotations are performed on the same physical direction.

To avoid these singularities, it becomes necessary to have two systems working on two different sets of Euler angles:

• one set of angles defined by three different indexes, which has the singularity condition on $\theta = (2n+1)\pi/2$;

• one set of angles where the first and the last indexes coincide, which has the singularity condition on $\theta = n\pi$;

with $n \in \mathbb{N}$. To merge these two systems and avoid singularities, there are two main options:

• run both systems all the time, get the attitude kinematics only from one system until it reaches its singularity condition on θ, then switch to the other system, which will be further from its singularity;

• run just one system at a time; when the system reaches its singularity condition, convert from the current set of angles to the other set through the attitude matrix, impose the calculated angles as initial condition on the other system, then start the integration from where it was interrupted, deactivating the system that reached the singularity.

Although the first option is simpler, the second option offers significant computational savings for the simulation. It is important to note that the kinematics model is only executed in the simulation to calculate the satellite's motion over time and is not executed on the satellite processor. Despite the added complexity of the system switch, the second option was chosen to accelerate the execution of the Simulink model.

In the model discussed in this report, the 312 and 313 sets of Euler angles were chosen. The equations for the integration and the conversion to attitude matrix are reported below:

$$\begin{cases} \dot{\phi}_{312} = \dfrac{\omega_z \cos\psi - \omega_x \sin\psi}{\cos\theta} \\ \dot{\theta}_{312} = \omega_x \cos\psi + \omega_z \sin\psi \\ \dot{\psi}_{312} = \omega_y - (\omega_z \cos\psi - \omega_x \sin\psi)\tan\theta \end{cases} \quad A_{312} = \begin{bmatrix} \cos\psi\cos\phi - \sin\psi\sin\phi\sin\theta & \cos\psi\sin\phi + \sin\psi\cos\phi\sin\theta & -\sin\psi\cos\theta \\ -\sin\phi\cos\theta & \cos\phi\cos\theta & \sin\theta \\ \sin\psi\cos\phi + \cos\psi\sin\phi\sin\theta & \sin\psi\sin\phi - \cos\psi\cos\phi\sin\theta & \cos\theta\cos\psi \end{bmatrix}$$

$$\begin{cases} \dot{\phi}_{313} = \dfrac{\omega_x \sin\psi + \omega_y \cos\psi}{\sin\theta} \\ \dot{\theta}_{313} = \omega_x \cos\psi - \omega_y \sin\psi \\ \dot{\psi}_{313} = \omega_z - (\omega_x \sin\psi + \omega_y \cos\psi)\cot\theta \end{cases} \quad A_{313} = \begin{bmatrix} \cos\psi\cos\phi - \sin\psi\sin\phi\cos\theta & \cos\psi\sin\phi + \sin\psi\cos\phi\cos\theta & \sin\psi\sin\theta \\ -\sin\psi\cos\phi - \cos\psi\sin\phi\cos\theta & -\sin\psi\sin\phi + \cos\psi\cos\phi\cos\theta & \cos\psi\sin\theta \\ \sin\phi\sin\theta & -\cos\phi\sin\theta & \cos\theta \end{bmatrix}$$

$$\tag{8}$$

In order to translate one set of Euler angles to the other set is sufficient to remember that A_{312} must be equal to A_{313}, since attitude matrices are both related to the same physical object. Inverting the formulas:

$$\begin{cases} \phi_{312} = \text{atan2}\left(-A^{2,1}, A^{2,2}\right) \\ \theta_{312} = \arcsin\left(A^{2,3}\right) \\ \psi_{312} = \text{atan2}\left(-A^{1,3}, A^{3,3}\right) \end{cases} \qquad \begin{cases} \phi_{313} = \text{atan2}\left(A^{3,1}, -A^{3,2}\right) \\ \theta_{313} = \arccos\left(A^{3,3}\right) \\ \psi_{313} = \text{atan2}\left(A^{1,3}, A^{2,3}\right) \end{cases} \qquad (9)$$

The system switcher has been designed in Simulink using basic boolean operators. These operators are combined to generate a 'flag' signal that selects the appropriate system, taking into account the singularity conditions of both. In more detail, the switcher logic takes as input three boolean signals:

- $|\cos\theta_{312}| < tol$, where tol is a chosen tolerance value to keep the 312 system distant from the singularity;
- $|\sin\theta_{313}| < tol$, where tol is a chosen tolerance value to keep the 313 system distant from the singularity;
- the **flag** of the system at the previous step time.

A truth table can be created using the given signals and expected output. The truth table can then be simplified using basic logic operators such as AND, OR, and NOT through boolean algebra. Finally, the logic can be implemented in the simulation to handle the activation of the two systems.

6. Disturbances analysis

In order to make a realistic simulation of the rotating motion of the spacecraft, the disturbances caused by the environment must be taken into account. The following paragraphs provide a brief introduction to the main disturbances acting on the system. The simulation results for the chosen satellite and orbit will then be presented to aid in the selection of the two most significant disturbances. Since the other disturbances are typically much smaller than the dominant ones (often by some orders of magnitude), they will be disregarded in the final simulation.

6.1. Magnetic Disturbance

The influence of the Earth's magnetic field on the satellite is relevant due to the proximity of the orbit taken in exam. Besides the crucial role that it plays in the actuation, the magnetic field could also cause big disturbances on the satellite's dynamics. The magnetic torque, whether generated by the magnetorquers or by parasitic currents present in the satellite, follows the general law:

$$\boldsymbol{M} = \boldsymbol{D} \times \boldsymbol{B} \qquad (10)$$

where $\boldsymbol{D}$ is the magnetic dipole generated by a coil or by parasitic currents, $\boldsymbol{B}$ is the magnetic field vector.

A mathematical model of the magnetic field is necessary to evaluate $\boldsymbol{B}$ given the satellite position along the orbit. The model chosen for the purpose is the 13th edition of the International Geomagnetic Reference Field (IGRF). According to this model, the magnetic field $\boldsymbol{B}$ is evaluated as the gradient of a magnetic scalar potential V, which is modelled as a spherical harmonic expansion of order N:

$$\boldsymbol{B}(r,\theta,\phi,t) = -\boldsymbol{\nabla}V(r,\theta,\phi,t) \qquad V(r,\theta,\phi,t) = a\sum_{n=1}^{N}\sum_{m=0}^{n}\left(\frac{a}{r}\right)^{n+1}\left(g^{n,m}(t)\cos m\phi + h^{n,m}(t)\sin m\phi\right)P^{n,m}(\cos\theta) \qquad (11)$$

where r,θ,ϕ are the spherical coordinates of the satellite in a Earth-Centered Earth-Fixed (ECEF) frame, a is the Earth's equatorial radius (6371.2 km), $P^{n,m}(\cos\theta)$ are the Gauss normalized associated Legendre functions, $g^{n,m}(t)$ and $h^{n,m}(t)$ are the Schmidt semi-normalized spherical harmonic coefficients. These coefficients are computed from experimental data and depend on time, as the Earth magnetic field is not constant but changes significantly every year. In this simulation, the coefficients refer to year 2020 of IGRF-13 and the expansion is computed up to order 13. Note that the model must be in the ECEF frame because the magnetic field rotates with the Earth. To adapt the model to an Earth-Centered Inertial (ECI) frame, a rotation matrix is required for the input and its transpose for the output. The matrix takes account of the angular velocity of Earth on time. Lastly, the magnetic field $\boldsymbol{B}$ can be expressed in the body frame through the attitude matrix.

Once that $\boldsymbol{B}$ is defined for every satellite position, the $\boldsymbol{D}$ vector is chosen as an arbitrary constant (based on typical microsat values) and the torque is easily computed along the orbit thanks to Equation 10.

6.2. SRP Disturbance

The Solar Radiation Pressure (SRP) torque is the disturbance generated by electromagnetic waves that impact on the spacecraft panels generating force. These forces acting on some of the panels can rise a net torque around the center of mass of the spacecraft. For this analysis, only the Sun radiation is considered, while a more rigorous study should also consider the infrared and the reflected Earth radiation. Moreover, no eclipse condition is analyzed during the simulation, which is a reasonable assumption given the SSO chosen in subsection 3.2.

The formula to calculate the force acting on each discrete panel i is the following:

$$F_i = -PA_i \left(\hat{S}_B \cdot \hat{N}_{B,i} \right) \left[(1 - \rho_s) \hat{S}_B + \left(2\rho_s \left(\hat{S}_B \cdot \hat{N}_{B,i} \right) + \frac{2}{3} \rho_d \right) \hat{N}_{B,i} \right] \tag{12}$$

In order to simulate this kind of disturbance, the coefficients of absorption ρ_a, specular reflection ρ_s and diffusion ρ_d must be decided. Since these three parameters are related through an energetic balance as $\rho_a + \rho_d + \rho_s = 1$, only two of them are indipendent while the third follows. These values clearly depends on the material of the main body and the solar panels of the spacecraft. In order to determine the force on each surface, the geometry of the panels of the satellite must be given (subsection 3.1), in particular the surface of each panel S_i and direction of the normal of the panel $\hat{N}_{B,i}$ expressed in $\mathcal{B}$ frame. The direction of Sun $\hat{S}_B$ is modeled in ECI frame considering the obliquity ϵ of Earth's rotation axis with respect to the ecliptic plane, then it is rotated in $\mathcal{B}$ frame through the attitude matrix.

Lastly, to be able to compute the torque it must be known where the resulting force acts on each panel (i.e. the centre of SRP force of the panel). It is assumed as a first approximation that the forces act on the geometric center of the corresponding plate. In order to correctly calculate the total torque, a shadow check must be performed. This has been implemented in Simulink by checking the sign of the dot product between the normal versor of the plate $\hat{N}_{B,i}$ and the Sun direction $\hat{S}_B$.

6.3. Drag Disturbance

Over extended periods, the spacecraft's engagement with the higher strates of Earth's atmosphere results in the generation of a torque around its center of mass. At altitudes less than 400 kilometers, the aerodynamic torque is usually the predominant factor, though its significance diminishes considerably beyond 700 kilometers of altitude. For the simulation, the geometry of the panels is defined in subsection 3.1. The coefficient of drag C_D is set to 2.2, the relative velocity considers both the rotation of Earth around its axis and the rotation motion of the spacecraft.

As for the SRP case (subsection 6.2), a sort of shadow check has been implemented based on the dot product between the relative velocity and the normal of the surface. This check is required since the modelling of the surface is composed of two faces, but only the external face impacts with the relative air movement. As for SRP torque, the position of the center of the force r_i should be evaluated for each panel. As a first approximation, the resulting force is placed in the geometric center of the panel.

$$M = \begin{cases} \sum_{i=1}^{n} r_i \times F_i & \text{if } \hat{N}_{B,i} \cdot \hat{v}_{B,i}^{rel} \geq 0 \\ 0 & \text{if } \hat{N}_{B,i} \cdot \hat{v}_{B,i}^{rel} < 0 \end{cases} \quad \text{with} \tag{13}$$

$$F_i = -\frac{1}{2} \rho C_D \|v_{B,i}^{rel}\|^2 \left(\hat{N}_{B,i} \cdot \hat{v}_{B,i}^{rel} \right) A_i \hat{v}_{B,i}^{rel} \qquad n = \text{number of faces}$$

The air density ρ is computed according to the US Standard Atmosphere of 1976. The model uses an exponential law to describe ρ as a function of altitude h:

$$\rho = \rho_0 \cdot \exp\left[-\frac{h - h_0}{H} \right] \tag{14}$$

Considering the orbit defined in subsection 3.2, the range of altitude is between 450 and 500 km. From this information, the constants of the formula are the following[4]:

$$\rho_0 = 1.585 \cdot 10^{-12} \text{ kg/m}^3 \qquad h_0 = 450 \text{ km} \qquad H = 60.828 \text{ km}$$

6.4. Gravity Gradient Disturbance

Since the gravity around the spacecraft is not uniform, a non-negligible gravity torque will arise from there. Studying the torque generated by an elementary force acting on the elementary mass dm the equation for this is obtained:

$$dM = -r \times \frac{Gm_t dm}{\|R + r\|^3} (R + r) \tag{15}$$

where r is the distance of dm from the center of mass and R is the distance of the center of mass from the center of Earth. Approximating this equation, and expressing the position vector of the centre of mass as the product of magnitude (R) with the direction cosines, it's possible to centre this torque in the principal inertia axes. Integrating this equation the final form is achieved.

$$M_x = \frac{3Gm_t}{R^3}(I_z - I_y)c_2 c_3$$

$$M_y = \frac{3Gm_t}{R^3}(I_x - I_z)c_1 c_3 \qquad (16)$$

$$M_z = \frac{3Gm_t}{R^3}(I_y - I_x)c_1 c_2$$

The c_1, c_2 and c_3 are the direction cosines of the radial direction in the principal axes. Therefore if one of the principal axes is aligned with the radial direction the torque will be zero because only one of the direction cosines is non-zero. It's clear that this disturbance acts in a continuous manner throughout the orbit motion and the torque produced depends mainly on the attitude matrix. Instead, the stability configuration depends on the distribution of mass of the spacecraft with respect to the orientation we want to achieve. For our case of study, inspired by the ESAIL mission from ESA, the satellite is nadir pointing. In particular the x_b direction has to be aligned with the nadir, while the z_b has to be normal with respect to the orbital plane. Using the numerical values of the spacecraft, and the orientation requirements just mentioned this particular configuration results unstable to GG disturbance.
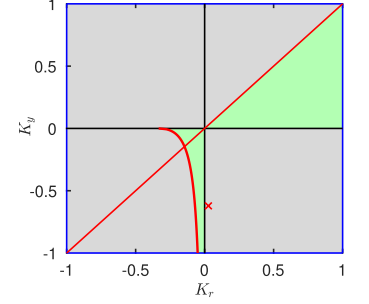

Figure 4: GG stability of satellite

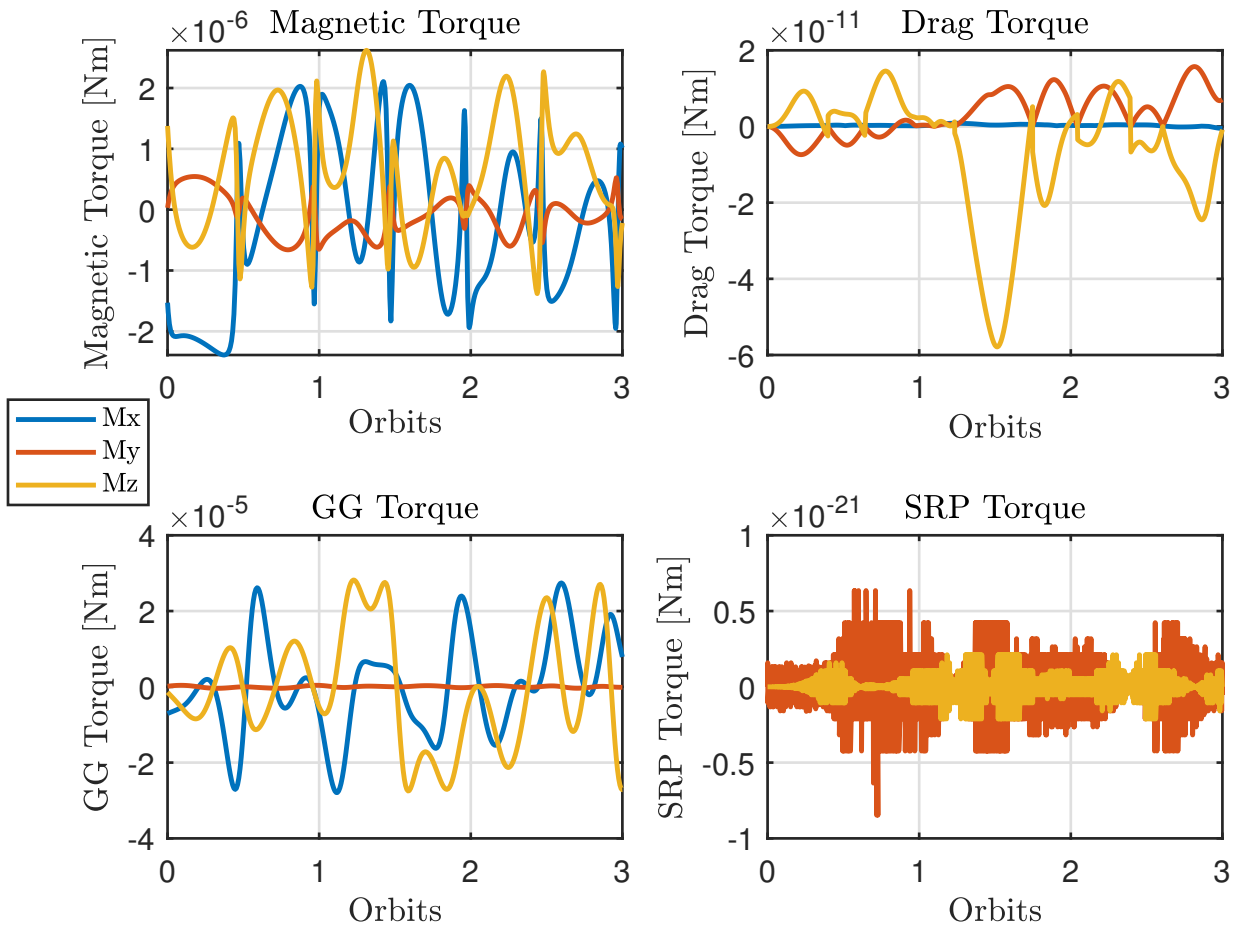## 6.5. Simulation of all disturbances

Figure 5: Simulation of all disturbances

The control-free motion has been simulated with all the disturbances for three full periods. The initial condition were set to null initial angular velocity and null Euler angles in the 312 set.

From the graphs of Figure 5 it is clear that SRP disturbance is negligible in our case, the graph shows only numerical zeros. In particular, this is due to the simmetry of the geometry of the spacecraft, a small set off for the CoM would have produced a net torque. It is clear, that in this specific case, the two most relevant disturbances are due to magnetic field interaction and the gravity gradient torque since the atmospheric drag torque is some orders of magnitude smaller.

Note that in the Gravity Gradient torque the y-axis component is almost null compared to the other components along x and z, this is due to the fact that the y-axis component of the torque depends on the difference between inertia moment along x and along z, for our case those two moments of inertia are very similar (see subsection 3.1).

7. Sensors

Sensors are fundamental tools that allows the SC to know its orientation or angular velocity. Their presence onboard is fundamental for having a controlled motion of the satellite. In this section, the 3 sensors used will be presented, it will be also clarified the motivation that lead the team to choose two additional sensors over the horizon sensor assigned.

7.1. Horizon Sensor

Horizon sensors are devices that can detect the centre of the planet, in our case Earth, and reconstruct the direction of that point with respect to the satellite. They usually work by analyzing the IR spectrum of the image through a thermopile to reduce the visible light spectrum interference caused by transition of day and night on earth. Due to the nadir pointing requirment a static earth sensor has been chosen for this specific application. In particular, the *Meisei Earth Horizon* was chosen, which has the following specifics:

$F.O.V.\,[deg]$	$Accuracy\,[deg]$	$Frequency\,[Hz]$
33	1	30

Table 3: Real data for Horizon Sensor

Due to operational requirements, the static sensor has to point the Earth, in particular the optical axis must have the same direction of the nadir (direction that links centre of earth and CoM of the S/C). To fulfill this request, a good option could be to position the sensor on the face that also contains the payload, that is the face of the spacecraft main body (cube) that has normal along the x_b direction.

The model implemented to simulate the behaviour of the sensor in the Simulink environment takes the real position of the S/C with respect to centre of Earth expressed in inertial space, changes its direction multiplying by -1 and expresses it in the $\mathcal{B}$ frame through the real attitude matrix $A_{B,N}$. This unit vector is the input of the sensor block, here it is sampled through a zero-order hold of frequency specified by Table 3 to simulate the digital nature of the sensor. Then some errors of measurments has to be added. It was decided to model two typical effects of real sensor: the mounting error that cause misalignment and also an accuracy error modeled with a band-limited white noise on all the components of the direction vector. Chronologically, first the misalignment is calculated, then the noise is introduced:

- The misalignment error was computed on Simulink by introducing a small deviation with respect to the nominal condition. This can be done by adding a small-scaled vector in the direction perpendicular of the unit vector that has to be measured. The scaling of this vector has to be small with respect to the unit direction considered as the measurment. Since the vector of the measured direction is initially unitary, the length of the bias vector introduced can be considered as $\tan \theta_{small} \approx \theta_{small}$, where θ_{small} represents the angle between real measurment and misaligned measurment. The θ_{small} selected is ...

- In the Simulink environment the white noise has to be defined through the power spectral density. This was selected as $N_p = \sigma^2 T_s$, where $sigma^2$ represents the variance as the standard deviation squared, while T_s is the sampling time of the sensor. It was decided to consider as standard deviation the value of $1\,deg$ (that is the accuracy from Table 3)

7.2. Magnetometer

Due to the LEO orbit and seen that from subsection 6.5 the magnetic field was considered as one of the main disturbances, it was thought that a magnetometer could have been a sensor to implement on-board the satellite. This kind of sensor are in general less accurate than optical sensor as sun sensor or star sensor, but since the magnetic field of LEO orbit is effectively enough strong, the sensor can provide always a measurment. Also, having a magnetorquer assigned as mandatory, the coupling of this actuator with a magnetometer can be exploited during the de-tumbling manuever since a direct dipole command is produced by the so-called *B-dot Control*, extensively discussed in section (...)

The fluxgate magnetometer typology is used, where for each body axis, two ferromagnetic cores are used parallel to the specific axis. The primary coil saturates the two bars alternatively in opposite direction, so that the secondary output theoretically can read a null induced voltage output produced by the time-varying flux. When external field is present, the symmetry of the alternate saturation is broken so that a shift on the magnetic flux of the secondary coil is produced. This net flux can be read by the time-history of a voltmeter on the secondary coil, since the spacing of the measured output voltage depends on the external magnetic field value.

Since magnetometer are usually characterized by low accuracy values, we searched for a high-accuracy and low-noise typology. The research of a suitable sensor opted for *MM200* furnished by *AAC ClydeSpace*. The following performance paramters characterize the sensor:

$N.S.D\,[nT/\sqrt{Hz}]$	$Frequency\,[Hz]$
1.18	< 500

Table 4: Real data for Magnetometer Sensor

For the Simulink model, the same approach of the Horizon sensor in subsection 7.1 has been used. In particular, the magnetic fiel vector from the block of subsection 6.1 has been trasnformed into the $\mathcal{B}$ reference frame through the attitude matrix from the true kinematics block section 5. This is the input vector that has to be sampled with a frequency specified by Table 4. For this case a range of frequencies can be chosen: we used the same frequency of the horizon sensor from Table 3 since it respects the constraint given by the magnetometer requirments.

Then the measurments errors have to be added, a first misalignment error modeled in the same way of the horizon sensor in subsection 7.1. For this case the perpendicular vector has been scaled by a factor of (...). The accuracy error, induced by the noise, has been modeled through a band-limited white noise added on each component. The value of the PSD is the square of the NSD presented in Table 4.

7.3. Sun Sensor

Sun sensors are devices that detect the position of the Sun by measuring the incidence angle of its radiation on a sensor surface. This surface is typically made of materials that can generate a current proportional to the intensity of the incident light. From the measure of the current I generated by the sensor surface of area S, knowing the intensity of the radiation W and the coefficient α of the sensor, the angle of the incident light θ is internally computed as:

$$I = \alpha S W \cos\theta \implies \theta = \arccos\left(\frac{I}{\alpha S W}\right) \tag{17}$$

The unit vector pointing towards the Sun can be easily computed by the sensor using the knowledge of two angles obtained by placing two surfaces on different directions on the same plane.

As discussed in section 3, the satellite mission consists in pointing the Earth on a Sun-synchronous orbit without any eclipse periods. Therefore, accuracy should be prioritised over having the best Field of View (FOV) when selecting the sensor. For this reason, the choice falls upon a small and light Fine Sun sensor with good performances such as the *AAC Clyde Space SS200*:

$F.O.V.\,[\text{deg}]$	$Accuracy\,[\text{deg}]$	$Frequency\,[Hz]$
90	0.3	30

Table 5: Real data for Sun Sensor

This sensor has to be placed in the same direction as the solar panels (i.e. in the z_b direction) so the Sun is constantly visible (since the orbit is Sun-synchronous). To avoid unnecessary complexity in the Simulink model, the sensor's field of view is not taken into consideration. This is because the sensor is not used during the detumbling manoeuvre, and in the tracking phase, the Sun is always visible. To simulate the output of the real sensor, the model uses the Sun direction calculated by adding the initial Earth-Sun vector to the position vector of the satellite in the inertial frame, which is computed through Keplerian dynamics. The resulting vector is then normalized, reversed, and transformed into the body frame using the attitude matrix. From here, errors have been added in the same manner as described for the horizon sensor (subsection 7.1).

8. Attitude determination

The problem of estimating the attitude matrix from the available measurements is central to spacecraft control. To determine the attitude of the spacecraft, the sensor models introduced earlier were used. The method used to determine the attitude is the SVD method, which has been developed whitin the framework of Wahba's problem. The latter consists in finding the orthogonal matrix which minimizes the weighted cost function

$$J(\boldsymbol{A_{BN}}) = \frac{1}{2} \sum_{i=1}^{N} \alpha_i \|\boldsymbol{s_i} - \boldsymbol{A_{BN}} \boldsymbol{v_i}\|^2 \tag{18}$$

in which $\{\boldsymbol{s_i}\}$ is a set of the N measured unit vectors in body frame and $\{\boldsymbol{v_i}\}$ the corresponding set of unitt vectors in the inertial frame, computed using the on-board models. The set of weights $\{\alpha_i\}$ was chosen based on the relative accuracy of each sensor. It was assumed that the weight vector $\underline{\alpha}$ is normalized to 1, i.e. $\sum_{i=1}^{N} \alpha_i = 1$. This method needs at least two available measurements, so it works also in the case that the Earth is outside the FOV of the horizon sensor.

Since $\boldsymbol{A_{BN}}$ is a orthogonal matrix and $\boldsymbol{s_i}$ and $\boldsymbol{v_i}$ are unit vectors, with some simple algebraic passages, the expression of J can be rewritten as:

$$J(\boldsymbol{A_{BN}}) = 1 - \sum_{i=1}^{N} \alpha_i (\boldsymbol{s_i}^T \boldsymbol{A_{BN}} \boldsymbol{v_i}) \tag{19}$$

The optimal solution minimizes J, therefore maximizes

$$\tilde{J}(\boldsymbol{A_{BN}}) = \sum_{i=1}^{N} \alpha_i (\boldsymbol{s_i}^T \boldsymbol{A_B} \boldsymbol{N} \boldsymbol{v_i}) = Tr(\boldsymbol{A_{BN}} \boldsymbol{B}^T) \tag{20}$$

where Tr is the trace operator and $\boldsymbol{B} = \sum_{i=1}^{N} \alpha_i \boldsymbol{s_i} \boldsymbol{v_i}^T$.

Since a direct solution is computationally expensive, a single value decomposition technique is used. The matrix B can be decomposed as:

$$\boldsymbol{B} = \boldsymbol{U}\boldsymbol{S}\boldsymbol{V}^T = \boldsymbol{U} diag([s_1 \quad s_2 \quad s_3])\boldsymbol{V}^T \tag{21}$$

U and V are orthogonal matrices, representing the matrices of eigenvectors of BB^T and $B^T B$ respectively, S is the diagonal matrix containing the square roots of the eigenvalues of $B^T B$. We can define the matrices

$$\boldsymbol{U_+} = \boldsymbol{U} diag([1 \quad 1 \quad det(\boldsymbol{U})]) \quad and \quad \boldsymbol{v_+} = \boldsymbol{V} diag([1 \quad 1 \quad det(\boldsymbol{V})])$$

Then

$$\boldsymbol{B} = \boldsymbol{U_+}\boldsymbol{S}'\boldsymbol{V_+}^T = \boldsymbol{B} = \boldsymbol{U_+} diag([s_1 \quad s_2 \quad s_3'])\boldsymbol{V_+}^T$$

where

$$s_3' = s_3 \det(\boldsymbol{U}) \det(\boldsymbol{V})$$

Now it can be defined the matrix W and its representation in terms of Euler axis/angle:

$$\boldsymbol{W} = \boldsymbol{U_+}^T \boldsymbol{A} \boldsymbol{V_+} = cos\theta \boldsymbol{I_3} - sin\theta[\boldsymbol{e} \times] + (1 - cos\theta)\boldsymbol{e}\boldsymbol{e}^T$$

$$Tr(\boldsymbol{A}\boldsymbol{B}^T) = Tr(\boldsymbol{W}\boldsymbol{S}') = \boldsymbol{e}^T \boldsymbol{S}'\boldsymbol{e} + cos\theta (Tr(\boldsymbol{S}') - \boldsymbol{e}^T \boldsymbol{S}'\boldsymbol{e})$$

The trace is maximized for $\theta = 0$, which gives $\boldsymbol{W} = \boldsymbol{I_3}$ and thus the optimal attitude matrix is

$$\boldsymbol{A} = \boldsymbol{U_+}\boldsymbol{V_+}^T = \boldsymbol{U} diag([1 \quad 1 \quad det(\boldsymbol{U})det(\boldsymbol{V})])\boldsymbol{V}^T$$

As previously mentioned, the weights required to construct the B matrix are determined by the relative accuracy of each sensor. As no data regarding the magnetometer's accuracy in degrees was provided, the following procedure was implemented to assess its relative accuracy and assign a weight to each sensor. A period of three orbits was simulated, assuming to be already in the tracking phase, in order to be sure to be in the FOV of the Earth horizon sensor. During the simulation it was computed the angle ϕ between the ideal unit vector and the measured one. For instance, when discussing the magnetometer, ϕ represents the angle between the unit vector parallel to the magnetic field and the unit vector measured by the magnetometer. For each sensor ϕ is a random number, it were then computed the expected value and the standard deviation with the formulas reported below

$$E[\phi] = \frac{1}{3T} \int_0^{3T} \phi \, dt \qquad \sigma_\phi^2 = \frac{1}{3T} \int_0^{3T} (\phi - E[\phi])^2 dt \qquad \sigma_\phi = \sqrt{\sigma_\phi^2}$$

where T is the period of the orbit. The integrals were evaluated numerically. The results obtained are reported in Table 6

Sensor	$E[\phi]$ [deg]	σ_ϕ [deg]
Magnetometer	0.0089	0.0078
Sun Sensor	0.3124	0.2720
Earth Sensor	1.1301	0.8544

Table 6: Expected value and standard deviation calculated

Basing on the previous results, it were chosen the weights reported in the next Table 7

Sensor	α_1 [−]	α_2 [−]
Magnetometer	0.80	0.80
Sun Sensor	0.15	0.2
Earth Sensor	0.05	−

Table 7: Weights α_1 and α_2

Since the attitude determination algorithm has been implement to work either if earth horizon measurments are not available, the α_2 weights are also calculated to fulfill the following requirement: $\sum_{i=1}^{N} \alpha_i = 1$.

9. Actuators

9.1. Magnetorquer

9.2. Reaction Wheels

Reaction wheels are one of the primary attitude control actuators for controlling the spacecraft, as they can give precise pointing and be controlled through feedback actively. They are based on acceleration and deceleration of spinning rotors. If the nominal condition is with a null angular velocity then that is a defining characteristic for reaction wheels as actuator.

Now, the equations for a dual spin satellite with no external torques applied are:

$$I_r \dot{\omega}_r = M_r$$

$$I_z \dot{\omega}_z = -I_r \dot{\omega}_r$$

The torque M_r is generated by an electric motor, which follows a characteristic performance curve. The general problem of control with reaction wheels can be modelled through the adequate set of Euler equations which contains the effects of the n actuators in the expression of the angular momentum:

$$\mathbf{h} = I\omega + \Delta\mathbf{h}_r$$

To simplify the solution of the control problem, considering the dynamics following the previous expression, we group the equation terms for determining the control torque required and the the effective control command for the reaction wheels:

$$I\dot{\omega} + \omega \times I\omega + \omega \times \Delta\mathbf{h}_r + \Delta\dot{\mathbf{h}}_r = \mathbf{T}$$

$$\mathbf{M}_c = -\omega \times \Delta\mathbf{h}_r - \Delta\dot{\mathbf{h}}_r$$

$$I_r \dot{\omega} = M_r$$

The equation for the evaluation of the control law, hence, stands as:

$$I\dot{\omega} + \omega \times I\omega = \mathbf{T} + \mathbf{M}_c$$

Once $\mathbf{M}_c$ is calculated using any suitable linear control design technique, $\mathbf{M}_r$ can be evaluated using the following procedure:

$$\Delta\mathbf{h}_r = -\mathbf{M}_c - \omega \times \Delta\mathbf{h}_r$$

$$\dot{\mathbf{h}}_r = -\mathbf{A}^*(\mathbf{M}_c + \omega \times \Delta\mathbf{h}_r)$$

Here $\mathbf{A}^*$ is the pseudo inverse matrix of $\mathbf{A}$ for the general case.

The Simulink implementation of the reaction wheel is performed by an input signal that is the required torque that the actuators should theoretically give. As previously mentioned, the reaction wheel must produce an angular acceleration to generate that torque on the satellite. Since the reaction wheel are physical objects, there are some saturation constraints on them. In particular, the producers specifies a maximum speed that can be reached and also a maximum torque that can be generated. Also, the actuator is affected by noise, for the analyzed case modelled as a band limited white noise.
The model chosen for the reaction wheels is the *OCE-RW40*, which is characterized by the following specifications:

$\omega_{max}\,[RPM]$	$\dot{h}_{max}\,[Nm]$	$\sigma_\omega\,[RPM]$
6000	0.1	2

Table 8: Real data for Reaction Wheel

All these real effects are modelled in the Simulink block of the reaction wheel.

10.   Control logic

The control logic of the satellite is implemented on the computer that handle all the on-board calculations. In particular, all the data from the in-FOV sensors has to be gathered. Then, based on the mission phase, the necessary control has to be calculated and a command has to be sent to the system of actuators. The necessary control calculation is discussed in this section. Clearly, every phase of the mission is somehow different, this could be due to the mission requirments (i.e. detumble or pointing) or to the physical equations that describe the problem (linear or non-linear). Also, when a phase of the mission has to be analyzed and a control applied to it, all the possibilities and limitations coming from sensors and actuators has to be evaluated. As a consequence, the design of a control logic is strictly related to the implementation of the actuators in the system, since even though a perfect control u can be designed by placing the fastest poles (in the linear case), then the actuator system will be highly penalized by not being able to perform that torque. As a consequence, it is important to bear in mind that when designing the control logic, always keep in consideration the actuators that will be used.
In the case under analysis, the magnetorquer actuators posses some useful and powerful proprerties, in particular when they are coupled with a magnetometer, the theory tells that the de-tumbling phase can be easily implemented[5]. On the other side, the control for a direction pointing (i.e. Nadir), in the case of magnetorquer is more difficult due to the unpleasent underactuated property of these magnetic systems. Infact, considering the equation of the actuator for the magnetorquer, and implementing that into the system equations, would result into a istantaneously uncontrollable system as cited in[6]. Nevertheless, by following the steps presented in[6], a fully magnetic actuated control can be reached but not without some effort and also drawbacks. In order not to complicate the next discussion, it was choosen the take into consideration also reaction wheels as a secondary actuator system.
In the next sub-sections the logic implemented in the Simulink environment will be presented, then all the more detailed actuator's cosniderations will be clarified.

10.1.   De-tumbling phase: the B-dot control

The De-tumbling phase is performed immediately after the release of the spacecraft by the launcher, at this moment the angular velocities are random and depends on the launcher motion, also the attitude is initally unknown. In order to make the satellite ready to enter in the operational regime, so that it can start the pointing of the sensor's targets and the payload, the spacecraft must be de-tumbled. This means to create a control that decelerate the rotational velocities and fetch them to arbitrarly small values.
A frequently adopted option on magnetic-actuated satellites is to implement the so-called *B-dot control*, this method allows to exploit magnetic measurments to produce a direct magnetic dipole command to the magnetorquer which at the end leads to arbitrarly small values of ω. The increasing interest on this kind of control law is due to the fact that magnetorquers posses very intersting propreties, such as[5]:

- absence of catastrophic failure modes (an example of this would be the RW actuators which were characterized by catastrophic failure due to electrostatic charge on the bearing);
- reliable architecture which leads to unlimited operational life;
- the possibility to smoothly modulate the control torque, without inducing coupling with flexible modes (when bang-bang techniques are not adopted);
- significant savings in terms of weight and complexity since no moving parts are present.

Instead, the major drawback of this kind of system is surely the underactuated property. In general the magnetorquer cannot provide an arbitrarly oriented control torque due to the physical law that rules this device.

$$M_c = D \times B_B \tag{22}$$

Clearly, it doesn't exist a D that satisfies the above equation if M_c and B are parallel. This implies to have, in general, a system that is not controllable at every istant, but it is in an averaged-sense. This implies a major difficulty in implementing a solely magnetic-actuated microsatellite. Avanzini et al.[5] demonstrate that asympotitc stability can be obtained through a law of this kind (using only magnetorquer and a magnetometer):

$$D = -\frac{k_\omega}{\|B_B\|}\dot{B}_B \tag{23}$$

The idea of this kind of command is that the variation in magnetic field B in the $\mathcal{B}$ frame can be written as:

$$\dot{B}_B = \frac{d\,(A_{B,N}B_N)}{dt} = \dot{A}_{B,N}B_N + A_{B,N}\dot{B}_N \approx \dot{A}_{B,N}B_N = -[\omega\times]A_{B,N}B_N = -[\omega\times]B_B \tag{24}$$

The approximation symbol is due to the fact that when $\omega \gg 1$, the variation of the magnetic field vector in $\mathcal{B}$ frame is mainly due to the rotation of the frame and less due to the changing of b_N (that is caused by the evolution in he orbital position and other slow variations due to geomagnetic field). With the above equation it has been demonstrated that ω and $\dot{B}$ are strictly related, so making the control law proportional to $\dot{B}$ would be similar to make it proportional to ω (like the 'standard' de-tumbling law). This mathematical considerations imply that for a detumbling law, it could be sufficient to have a magnetometer and a magnetorquer without a direct measurment of the angular velocity obtained by a gyro. Another positive consequence of having a proportional law that produces directly a magnetic dipole D, is that the command is directly make as an input of the actuator (without inverting any actuator law). It is important to underline that this kind of law would work at his best when angular velocity is high enough to make the assumption of Equation 24 true. In theory the acutated torque is:

$$M_c = -\frac{k_\omega}{\|B_B\|}\dot{B}_B \times B_B \tag{25}$$

also notice that when $\omega \gg 1$ Equation 24 is more and more true, and so B_B and $\dot{B}_B$ are perpendicular, resulting in the maximum actuable control torque.

Regarding the control law Equation 23, it has to be seen that the vector derived is not the derivative of the magnetic field vector, but it is the derivative of the unit vector of the direction of the magnetic field. Also, notice that all the vector in the above relationship are in the $\mathcal{B}$ frame since the magnetic field vector B comes from the magnetometer measurment.

In the context of the simulation environment on Simulink, the formulation choosen for the b-dot control comes from[5] of Avanzini et Al. Some precaution has to be taken when implementing the law, since the numerical derivative of a mesaured (hence noisy) signal has to be performed. This inconvinence can be overcome by using a low-pass filter[7]. In order to make some sense out of the calculation, a discrete low-pass Butterworth filter of the 1st order has been used just after the discrete derivative block. Setting the cut-off frequency on 0.06 rad/s the signal is pretty clean and the results of simulation are coherent

10.2. Slew and Nadir pointing phases

10.2.1 Control law for the Slew and Tracking Manuever

The goal for the control system at this phase of the mission, is to track the $\mathcal{LVLH}$ frame. In order to obtain the right alignment of the frames, both the attitude error and the angular velocity error should be zero. Infact the tracking of the $\mathcal{LVLH}$ frame means not only to reduce the error angles but also to arrive at the aligned condition with the correct angular velocity in order to not overshoot the correct position. In this case of control, the attitude error matrix is A_{BL}, which leads from the $\mathcal{LVLH}$ to the body frame, and the goal is to make it close to the identity matrix. For this reason, it was desired to make the extra diagonal terms close to zero and the error vector was defined as

$$\alpha = (A_{BL}^T - A_{BL})^V$$

The $[\cdot]^V$ operator is the inverse of $[\cdot\times]$, so it maps a skew-symmetric matrix back to its generating vector. The angular velocity error was defined as

$$\omega_{BL} = \omega - A_{BL}[0\ \ 0\ \ n]^T$$

$\vec{\omega}$ was obtained by taking the numerical derivative of the matrix A_{BN}, the matrix computed with the attitude determination algorithm, and then inverting the formula

$$\dot{A}_{BN} = -[\omega\times]A_{BN} \tag{26}$$

Since A_{BN} is affected by noise, taking its derivative numerically amplifies it, leading to a bad estimation of the angular velocity. Therefore a discrete lowpass Butterworth filter was applied before the computation of ω. This was set as a 1st order filter with cut-off frequency at 1 rad/s. Once computed α and ω_{BL} a suitable control law was:

$$M_c = -k_p\alpha - k_d\omega_{BL}$$

This kind of control law is inspired by the linear full-state feedback control $u = -kx$. In particular, referred to the linearized Euler equations in which a set of three Euler angles $\alpha = (\alpha_1 \alpha_2 \alpha_3)$ is introduced. This set of small angles represent the misalignment between the $\mathcal{B}$ and $\mathcal{LVLH}$ frame. When this linearization is made, the state x for the state-space formulation, contains α and $\dot{\alpha}$. If the $u = -kx$ is implemented with that state, the control law becomes a *Proportional-Derivative* control, in the form:

$$M_c = -K_p \alpha - K_d \dot{\alpha}$$

Since the linear control theory allows to use different metholodgies to caluclate the gains matrices k_p and k_d, the linearized control law was firstly analyzed. In particular, the pole placment technique was used, on the following state-space representation of the system.

$$\begin{cases} \dot{x} = Ax + Bu \\ y = Cx + Du \end{cases} \quad A = \begin{bmatrix} 0 & (1-K_x)n & 0 & -n^2 K_x & 0 & 0 \\ (K_y-1)n & 0 & 0 & 0 & -n^2 K_y & 0 \\ 0 & 0 & 0 & 0 & 0 & 0 \\ 1 & 0 & 0 & 0 & 0 & 0 \\ 0 & 1 & 0 & 0 & 0 & 0 \\ 0 & 0 & 1 & 0 & 0 & 0 \end{bmatrix} \quad B = \begin{bmatrix} \frac{1}{I_x} & 0 & 0 \\ 0 & \frac{1}{I_x} & 0 \\ 0 & 0 & \frac{1}{I_x} \\ 0 & 0 & 0 \\ 0 & 0 & 0 \\ 0 & 0 & 0 \end{bmatrix} \quad (27)$$

The open-loop poles caluclated for this system are:

$$p_{open} = \begin{bmatrix} 0 \pm 0.0011i \\ 0 \pm 0.0002i \\ 0 \end{bmatrix} \quad (28)$$

The gain matrix $K = [K_d \ K_p]$ is assesed through the the *place(A,B,p)* Matlab function that requires the state-space matrices A and B, and also the closed-loop poles that are desired p. At this point, this vector of six poles must be hypotized. Some precatuions must be taken when the poles are decided:

- closed-loop poles shall not be too far from the corresponding open-loop poles, since there are constraints on the capabilities of the actuator;
- the real part of the closed-loop poles must be negative in order to guarantee asymptotic stability;
- the imaginary part of the poles should be decided in order to minimize the overshoot;

The chosen poles are:

$$p = \begin{bmatrix} -0.02 \pm 0.1i \\ -0.01 \pm 0.06i \\ -0.05 \pm 0.1i \end{bmatrix} \quad (29)$$

The gain matrix can be used for the linear-control law. For simplicity, it wasn't used a matrix for the non-linear control but only a scalar, in particular it was selected the order of magnitude of the gain matrix from linear control just calculated. The values for the gains were then refined with trial and error. The response of the system was satisfactory with the following values:

$$k_p = 0.001 \qquad k_d = 0.6$$

10.2.2 Actuator command logic for Slew and Nadir pointing

Once the control torque M_c has been calculated, a logic was implemented to translate it into a command to be sent to the actuators. Magnetic actuators generate the torque with the formula

$$M = -[B \times]D \quad (30)$$

where $[B \times]$ is the skew symmetric matrix obtained applying the $[\cdot \times]$ operator to the magnetic field vector in body frame, measured by the magnetometer. However, it isn't possible to compute D by inverting Equation 30 because $[B \times]$ is singular. This reflects the fact that is never possible to generate three independents components of the control torque, since M is always perpendicular to both D and B. One possible solution is to add one or more reaction wheel(s). It was chosen to add two reaction wheels, one along x_B and one along y_B of the $\mathcal{B}$ frame. This because, as it is shown in Equation 32 and Equation 33, when only one reaction wheel is used, the matrix of the linear system necessary to be solved, becomes singular when the component of the magnetic field aligned with the reaction wheel is zero. As shown in Figure 6 all components of the magnetic field will go to zero at a certain point. If just one reaction wheel would be used, it should be disactivated when the respective component of B goes to 0. This would mean that at certain istants of time, the only actuators that can operate are the magnetorquer. This would lead to the undeterminate problem of defining a command to the magnetoactuator Equation 23.

Following the considerations given just above, the command is always given in the form:

$$\boldsymbol{cmd} = [D_x \ D_y \ D_z \ -\dot{h}_x \ -\dot{h}_y]^T \tag{31}$$

where D_x, D_y and D_z are the dipoles to be given by the magnetic actuators, $\dot{h}_x$ and $\dot{h}_y$ are the moments to be given by the reaction wheels.

Only one reaction wheel is used at a time, they are never used all at once. A logic was implemented to choose which reaction wheel to use. It consists in an if/else construct, implemented in Simulink through two enabled subsystems, which takes as condition that $|B_x| \geq 10^{-5} \ T$. If the condition is satisfied, the reaction wheel along x is used and the linear system reported below is solved,

$$\begin{bmatrix} 1 & B_z & -B_y \\ -B_z & 0 & B_x \\ B_y & -B_x & 0 \end{bmatrix} \begin{bmatrix} -\dot{h}_x \\ D_y \\ D_z \end{bmatrix} = \begin{bmatrix} M_x \\ M_y \\ M_z \end{bmatrix} \tag{32}$$

The command vector is assembled as indicated in Equation 31 by taking the solution Equation 32 and setting to zero D_x and $\dot{h}_y$. If the condition is not satisfied, the reaction wheel along y is used, the linear system to be solved is

$$\begin{bmatrix} 0 & B_z & -B_y \\ -B_z & 1 & B_x \\ B_y & -B_x & 0 \end{bmatrix} \begin{bmatrix} D_x \\ -\dot{h}_y \\ D_z \end{bmatrix} = \begin{bmatrix} M_x \\ M_y \\ M_z \end{bmatrix} \tag{33}$$

and the command vector is assembled as indicated in Equation 31 by taking the solution ofEquation 33 and setting to zero D_y and $\dot{h}_x$. The idea behind this kind of logic was to be always able to compute the command vector. Indeed, the matrix of Equation 32 is singular when $B_x = 0 \ T$ and the matrix of Equation 33 is singular when $B_y = 0 \ T$. It is clear that, using this kind of logic, it is always possible to compute a command to be sent to the actuators. The assumption that was made is that at every instant of time, at least one of B_x and B_y is non zero. Looking at the graph in figure Figure 6, it can be noticed that, when B_x is zero, B_y is far from zero and vice-versa. It wasn't chosen to put the second reaction wheel along z axis because, as it is shown in the graph reported in the same figure, there are instant of times along the orbit during which both B_x and B_z are null or both B_y and B_z are null.
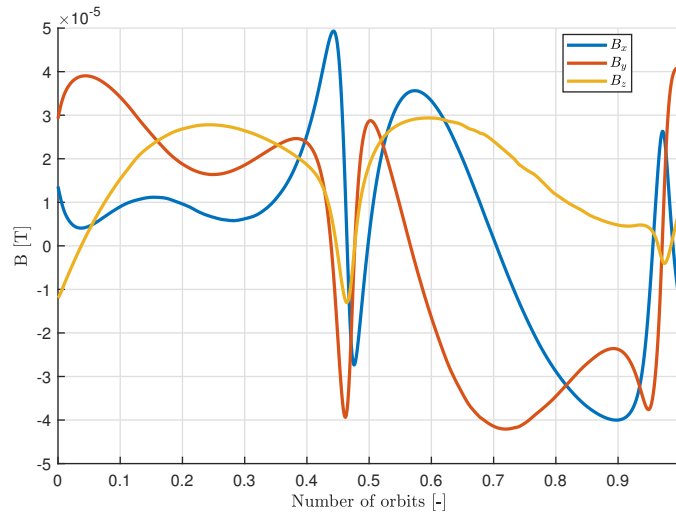

Figure 6: Magnetic Field in $\mathcal{B}$ frame

Bibliography

[1] ESA. Esail maritime satellite launched. Website, 2020. Site: `https://www.esa.int/Applications/Connectivity_and_Secure_Communications/ESAIL_maritime_satellite_launched`.

[2] Howard D. Curtis. *Orbital Mechanics for Engineering Students*. Elsevier, 2014.

[3] ESA. Types of orbits. Website, 2020. Site: `https://www.esa.int/Enabling_Support/Space_Transportation/Types_of_orbits`.

[4] James R. Wertz. *Spacecraft Attitude Determination And Control*. Kluwer Academic Publishers, 1978.

[5] Giulio Avanzini, Fabrizio Giulietti. Magnetic Detumbling of a Rigid Spacecraft. *Journal of Guidance, Control and Dynamics*, 35(4):1326–1333, 8 2012.

[6] M. Lovera, A. Astolfi. Spacecraft attitude control using magnetic actuators. *Elsevier*, 40(4):1405–1414, 2 2004.

[7] John l. Crassidis F. Landis Markley. *Fundamentals of Spacecraft Attitude Determination and Control*. Springer, 2014.